JOURNAL OF PROPULSION AND POWER
Vol. 22, No. 1, January–February 2006

Visualizations of Gas-Phase NTO/MMH Reactivity

Laurent Catoire,* Nabiha Chaumeix,† Servane Pichon,‡ and Claude Paillard§
Laboratoire de Combustion et Systèmes Réactifs (LCSR)—Centre National de la Recherche Scientifique (CNRS) and University of Orléans, 45071 Orléans Cedex 02, France

The objectives of this investigation are to study the details of the nonignition, preignition, ignition, and combustion sequences of the NTO (nitrogen tetroxide)/MMH (monomethyl hydrazine) bipropellant combination. Several techniques have been used to visualize NTO/MMH reactivity at room temperature and recreate some failure scenarios. NTO/MMH flammability diagrams have been established experimentally.

Introduction

THE NTO (nitrogen tetroxide)/MMH (monomethyl hydrazine) bipropellant combination is frequently used for propulsion, attitude control, and altitude control of satellites, missiles, and launchers.[1,2] Despite these numerous applications, the ignition chemistry of the hypergolic NTO/MMH system and the features of the corresponding ignition process are far from being understood, especially at room temperature (about 293 K) and below. Recently we proposed a detailed chemical kinetic model that could explain both the gas-phase hypergolic NTO/MMH ignition (transient regime) and the NTO/MMH combustion (permanent regime).[3] This model can also be used to interpret nonignition cases. This model was built based on naked-eye observations, various chemical analyses, and deductions from experimental results obtained by using more or less sophisticated experimental techniques.[4–24] However, no high-speed visualization of the NTO/MMH reactivity has previously been presented. One aim of this study is to present a direct visualization of the gas-phase NTO/MMH reactivity at room temperature. The current explanation for NTO/MMH hypergolic ignition can benefit from the information provided by visualization, and, in general, visualization is very important for combustion modeling purposes. Among the hydrazine family of compounds (hydrazine, monomethylhydrazine, and asymmetrical dimethylhydrazine), direct visualization has only been performed for the hydrazine/NTO combination. That study revealed that the ignition takes place in the gas-phase above the liquids when liquid hydrazine and liquid NTO come into contact.[6] Nevertheless, that study did not focus on the details of the gas-phase hydrazine/NTO ignition and therefore these details have never been visualized.

The other aim of this study is to establish experimental flammability diagrams obtained from the visualization study. This is of interest fundamentally for propulsion purposes and also for the examination and prevention of propellant vapor mixing between the check valves in bipropellant pressurization systems.

Experimental

The study has been performed at room temperature with various experimental apparatuses, but always in the same basic way: a jet of NTO (pure or diluted by helium) is introduced in a spherical metallic bomb or spherical glass vessel that contains gaseous MMH (pure or diluted). The jet of NTO is obtained when NTO, at a static pressure P_2, is allowed to expand into the vessel containing MMH at a static pressure P_1. P_1 and P_2 are measured when the two gases (or gaseous mixtures) are at rest. Several optical techniques have been used to follow NTO/MMH reactivity. Experiments were recorded with a Kodak EKTAPRO HS 4540 digital high-speed camera, capable of recording at up to 4500 frames per second. The frames were transferred to a personal computer and then processed with VISILOG 5.2 image processing.

Results and Discussion

Visualization of the NTO/MMH Reactivity Without Ignition

Previous studies showed the formation of products, appearing as a white-yellow fog, when the two gases come into contact without ignition. This product formation is visible to the naked eye and appears almost instantaneously. Based on UV spectrophotometry measurements (not shown here), this formation seems to be complete in less than 100 ms. This product formation seems to be unavoidable and is observed even if the two gases are both highly diluted (up to 97 mol% He). The experimental setup used for the visualization is described in Ref. 25. Briefly, the bomb is a stainless-steel sphere (i.d. 250 mm) equipped with two quartz windows (70 mm in diameter, 40 mm thick). The light source is a white continuous lamp. Figure 1 shows what is observed when a jet of NTO is introduced in a spherical metallic bomb, which contains gaseous MMH. Time zero for Fig. 1 is the time when the valve separating the NTO and MMH is opened. The introduction is made at the top of the figure. MMH does not absorb in the 400–800-nm wavelength range. Figure 2 shows that NTO does not absorb all of the wavelengths of the incident light and that Fig. 1 cannot be interpreted in terms of absorption of the light by NTO. Figure 1 shows that the formation of the product species occurs on a time scale of tens of milliseconds. The kinetics of formation of these products is not only dependent on the chemical kinetics but also depends strongly on the characteristics of the jet: P_1, P_2, the ratio P_2/P_1, and the inner diameter of the tube through which the NTO is introduced. For instance, the formation of the fog seems to be homogeneous over the whole visible volume in Fig. 1, but for different values of P_1 and P_2, this is no longer the case, as shown in Fig. 3. The way these species form is probably important for ignition. It is often thought that the species formed inhibit ignition by consumption of reactants. This conclusion is logically drawn from the naked-eye experimental observation that a fog forms when NTO/MMH does not ignite. However, a detailed chemical kinetic study shows that these products may form in all cases, whether or not ignition occurs, and that the exothermic formation of these products may actually promote ignition. However, the same study shows that hypergolicity can be explained without the formation of these species. Under some conditions, the formation of these species plays the role of an ignition source that renders some NTO/MMH mixtures hypergolic that would not be predicted to be hypergolic if these species did not form.

Received 28 May 2004; revision received 19 May 2005; accepted for publication 15 May 2005.

*Doctor, Assistant Professor, 1C, av. de la Recherche Scientifique.
†Doctor, Senior Researcher, 1C, av. de la Recherche Scientifique.
‡Doctor, 1C, av. de la Recherche Scientifique.
§Professor, 1C, av. de la Recherche Scientifique.

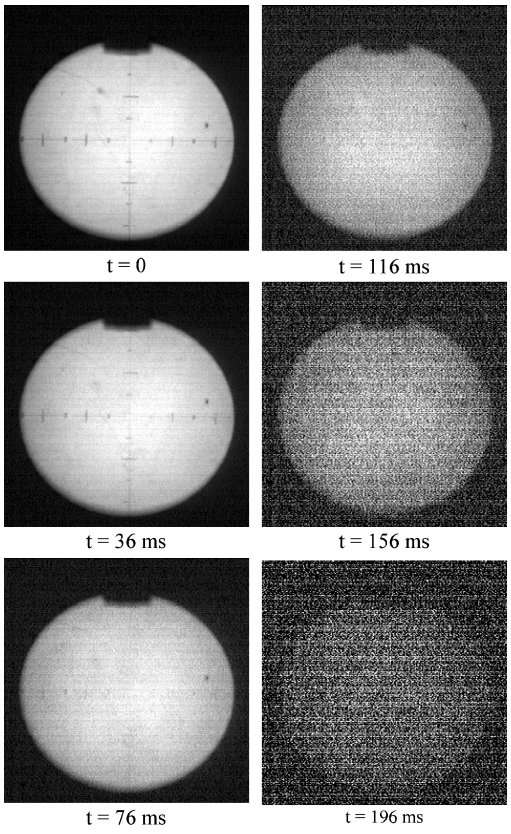

Fig. 1 Typical visualization of the products formation when MMH and NTO come into contact at room temperature (293 K). $P_1 = 9.33$ kPa (80 mol% He + 20 mol% MMH) and $P_2 = 160$ kPa (pure NTO). Frames per second: 250. NTO is introduced at the top of the spherical vessel.

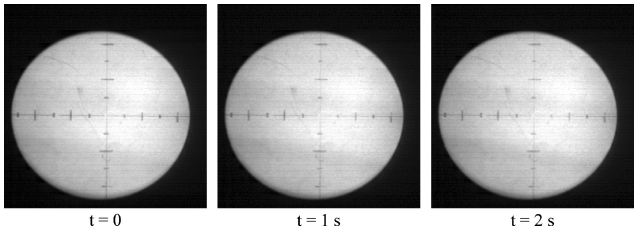

Fig. 2 Experiment showing that pure NTO is not able to absorb the incident white light. At time zero, the spherical bomb is initially empty.

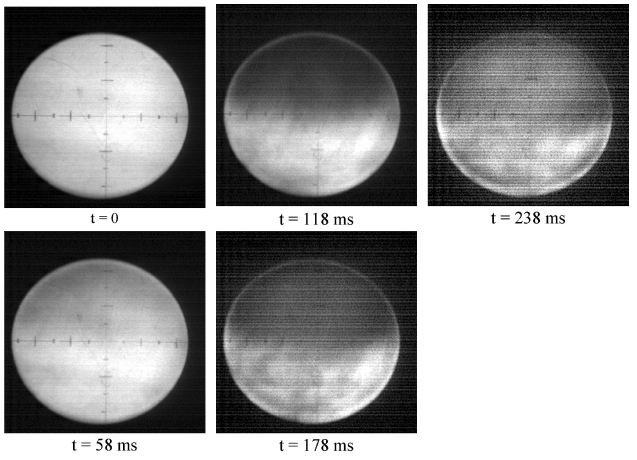

Fig. 3 Inhomogeneous fog formation when MMH and NTO come into contact at room temperature. NTO is introduced at the top of the spherical vessel. $P_1 = 2$ kPa (80 mol% He + 20 mol% MMH), $P_2 = 102.4$ kPa (pure NTO). Frames per second: 500.

Schlieren Visualization of the Preignition Reactivity, Schlieren Visualization of the Ignition, and Schlieren Visualization of the Flame

The question of whether the product species that lead to visible fog formation also form during the preignition period is interesting. The answer allows the validation of the NTO/MMH detailed kinetic model, which predicts that preignition products also form when ignition occurs. Because the observation of what happens during the preignition period cannot be made by direct unassisted observation, other techniques have been or have to be used to assess the formation of preignition products, and direct visualization is of primary importance. The optical technique used to obtain Figs. 1 and 3 is in fact interesting for the visualization of the fog but it does not allow a good visualization of the preignition reactivity because the high intensity of the light source can prevent the visualization of the preignition products in the early stages of their formation.

The technique used here is Schlieren visualization. The characterization and analysis of flame shape and position from Schlieren images has provided an effective method for studying combustion processes. The Schlieren technique is based on the angular deflection undergone by a light ray when passing through a gas characterized by refractive-index inhomogeneities created by density or temperature variations or chemical-composition variations. In fact, here both density gradient (mixing NTO/MMH and fog formation) and temperature gradient (exothermic formation of the fog) are likely. The experimental setup consists of two concave hemispherical mirrors (100 mm in diameter, focal length of 0.5 m). The light source is a white continuous lamp focused to a point with two lenses. The bomb is exactly the same as used for the visualization of the formation of the fog. Time zero for Fig. 4 is the time when the valve separating NTO and MMH is opened. Figure 4 shows what is observed with this technique when ignition is observed. The dynamic visualization is more spectacular than the images given in Fig. 4, but the frames are much more meaningful. Comparisons between visualizations in the nonignition and ignition cases allow for interpretation of the images. Frames from time zero up to about time 1.1–1.2 s show the formation of the fog, which appears as filaments probably at the interface of the two gases. This fog accumulates as shown by the images from time $t = 792$ ms up to times $t = 1112$ ms and $t = 1232$ ms. Then, at about $t = 1232$ ms, combustion begins. This is indicated by the darkest zones of the gaseous volume. These are not observed in cases where ignition does not occur.

Direct Visualization of NTO/MMH Hypergolic Ignition/Combustion

In these experiments, the hypergolic ignition has been studied by the visualization of the NTO/MMH flame. The corresponding experimental setup is shown in Fig. 5. No light source is needed for these experiments. The vessels are made of Pyrex® glass. The vessel in which the reaction takes place (noted 1 in Fig. 5) has a volume of 1 L and a surface/volume ratio of 48 m^{-1}. In a dark room, a jet of NTO (pure or diluted by helium) is introduced into a spherical glass bomb that contains gaseous MMH (pure or diluted by helium). The jet of NTO is obtained when NTO, at a static pressure P_2, is allowed to expand into the vessel containing MMH at a static pressure P_1. Ignition and nonignition have been observed, depending on dilution, pressure P_2, pressure P_1, and the ratio P_2/P_1. When ignition occurs, a dazzling white-yellow flash is visible to the naked eye. High-speed visualization has also been performed for these experiments.

A typical sequence of frames is shown in Fig. 6. In this case, time zero is taken to be the time when the first light emission is observed, because mixing and preignition product formation are not visualized in these experiments. For the case shown in Fig. 6, ignition and combustion occur over a time period of about 100 ms. Two sequences of light emission are generally observed, as seen in Fig. 6. The first light emission appears to originate from the whole gas volume, just as the prereaction product formation does, whereas the second light emission is much more localized and looks like a flame. As the formation of the fog as described previously does not exhibit chemiluminescence, this seems to show that

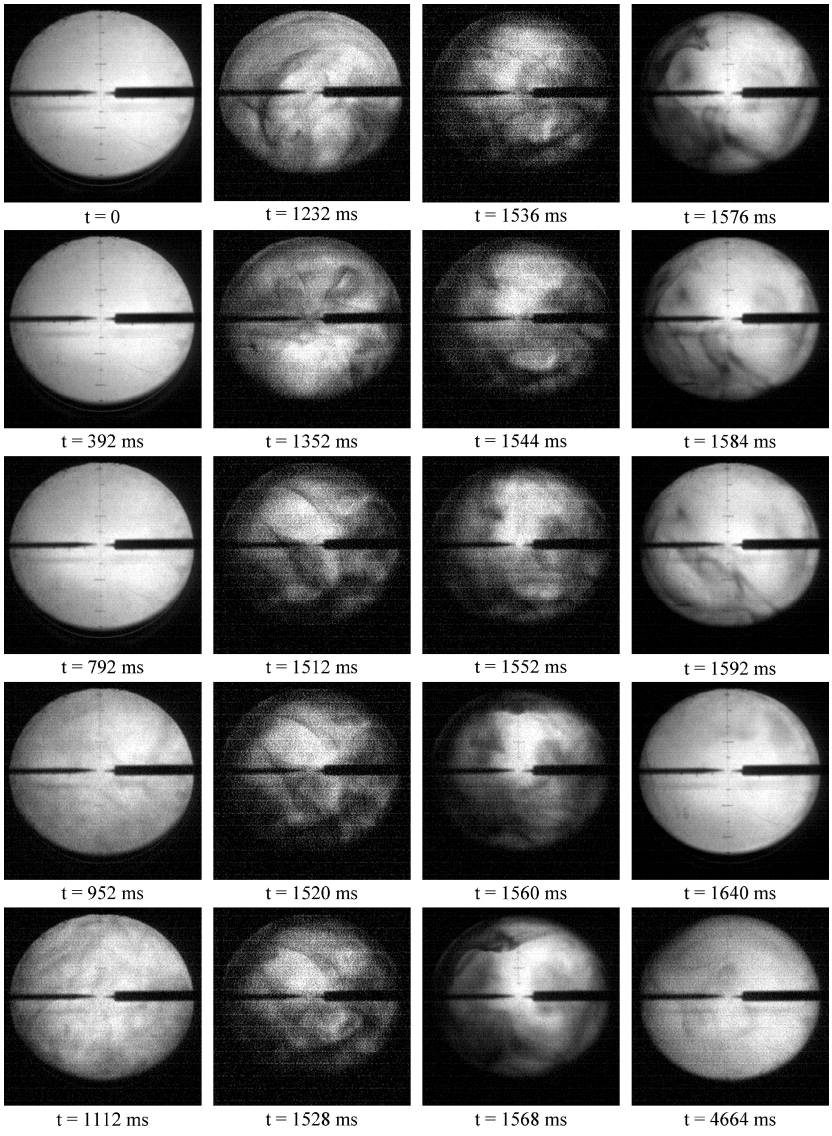

Fig. 4 Schlieren visualization of NTO/MMH hypergolic ignition at room temperature. $P_1 = 7.73$ kPa (75 mol% Ar + 25 mol% MMH) and $P_2 = 30$ kPa (pure NTO).

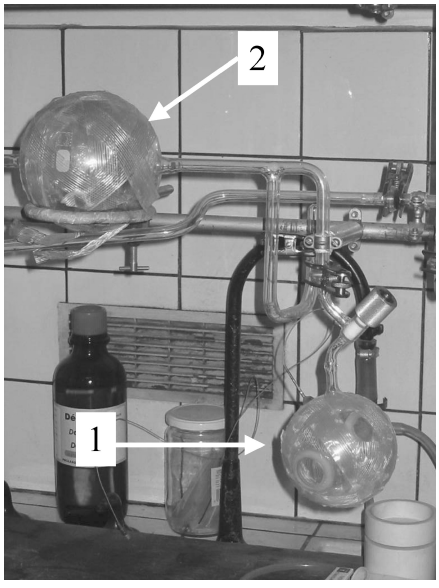

Fig. 5 Experimental setup used for the direct visualization of NTO/MMH ignition.

the observed chemiluminescence is due to reactions induced by the exothermicity that accompanies the formation of the fog when formed in sufficient quantities. Therefore, the second light emission appears to be very dependent to the initial exothermicity and to the radicals produced. All these observations are fully consistent with the detailed kinetic model, which often predicts two-step ignition. A situation between nonignition and two-step ignition is one-step light emission, that is, only the first light emission. Such a situation is probably illustrated by Fig. 7, in which a light emission very similar to the first light emission of Fig. 6 but not followed by a second light emission is shown. Such a situation could lead either to ignition or to nonignition depending on the experimental conditions, in particular the adiabaticity or nonadiabaticity of the vessel in which the reaction takes place.

NTO/MMH/He Flammability Diagrams

These observations can be rationalized in terms of flammability-limit diagrams. Figure 8 presents the boundary between no ignition risks (fog formation without chemiluminescence) and ignition risks. P_2 and P_1 flammability diagrams have been established for various conditions of P_1, P_2, ratio P_2/P_1, and dilution by helium (see Figs. 8–11). Helium is considered here because it is the most common choice for bipropellant pressurization systems. For these diagrams, all luminous events have been considered as indications that

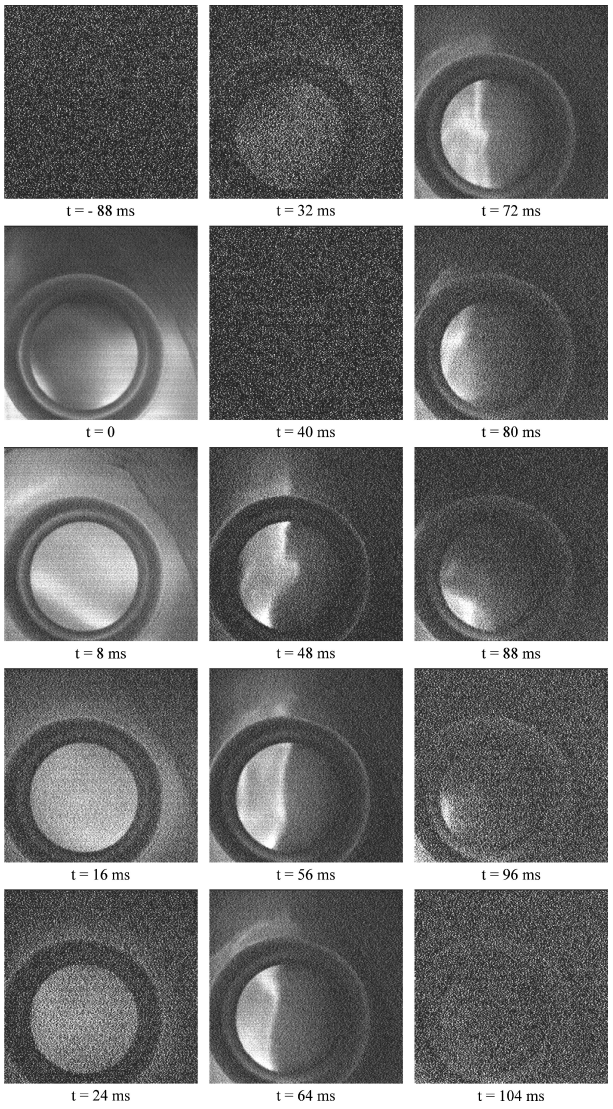

Fig. 6 Direct visualization of NTO/MMH hypergolic ignition and combustion in the spherical glass vessel at room temperature. $P_1 = 5.33$ kPa (70 mol% Ar + 30 mol% MMH) and $P_2 = 60$ kPa (pure NTO). Frames per second: 125.

the "mixture" considered is potentially hazardous. The occurence of invisible flames has also been examined by using UV spectrophotometry to follow the nonignition, preignition and ignition events, because it is possible to detect unambiguously ignition and nonignition from the UV absorption signals, as shown in Fig. 12, even if the light emission is invisible. It appears that ignition without light emission in the visible spectral range is an exception and that emission in the visible spectral range (400–800 nm) always accompanies emission at 320 nm. No ignition has been observed when the volumic percentage of helium is 85 for $20 < P_2$ (kPa) < 90 and $3 < P_1$ (kPa) < 16. Although interesting, the diagrams shown in Figs. 8–11 do not allow for a straightforward interpretation in terms of the reaction mechanism and chemical kinetics of ignition. The use of these diagrams is also not straightforward because some of the (P_2, P_1) conditions above the limit are probably not hazardous (for instance, very high P_2 for a given P_1 can hardly be hazardous because very lean mixtures are formed). Other diagrams are possible with some assumptions. By assuming rapid isothermal mixing when one volume expands in the other, it is possible to define an initial total pressure and an initial $MMH/NO_2/N_2O_4$/He composition. With these assumptions, the final pressure P of the mixture is given by

$$P = \frac{P_1 V_1 + P_2 V_2}{V_1 + V_2}$$

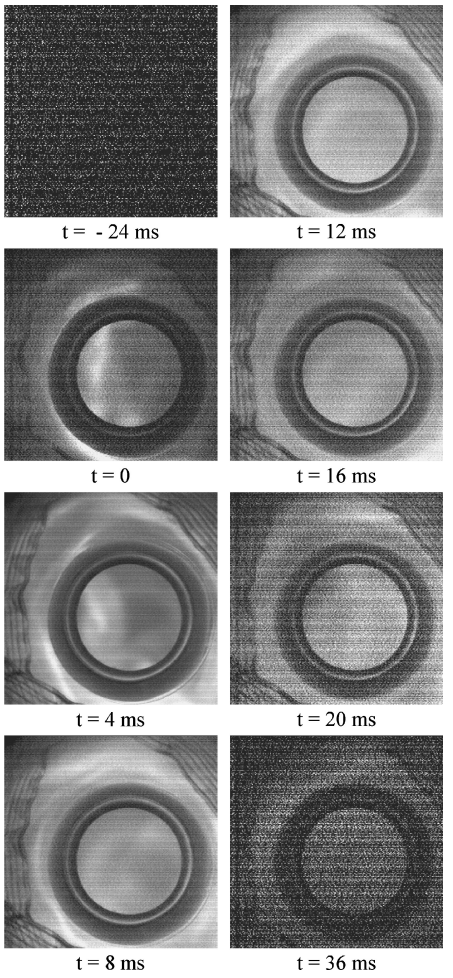

Fig. 7 Direct visualization of NTO/MMH hypergolic ignition and combustion in the spherical glass vessel at room temperature. $P_1 = 5.33$ kPa (70 mol% Ar + 30 mol% MMH) and $P_2 = 40$ kPa (pure NTO). Frames per second: 250.

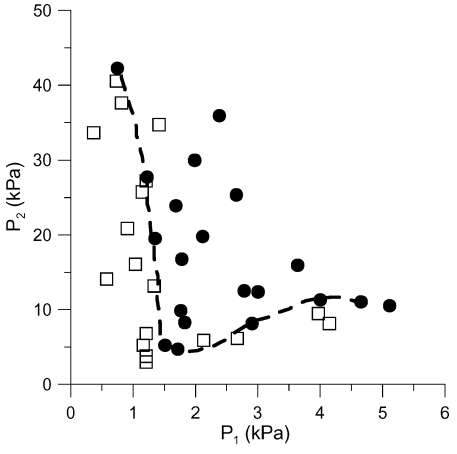

Fig. 8 NTO/MMH flammability diagram at room temperature (295 K). P_1 = mixture 53 mol% He + 47 mol% MMH. P_2 = mixture 53 mol% He + 47 mol% NTO. S/V = 48 m^{-1}. □, no ignition; ●, ignition.

This is reasonable if, as appears to be the case from the visualizations, the time scale for mixing is shorter than the time scale for ignition. The proportions of NO_2 and N_2O_4 in NTO are determined from equilibrium thermodynamics. NO_2–N_2O_4 equilibrium is reached, at the temperatures and pressures considered, in a few milliseconds. This represents a negligible time compared to reaction times. Then, by considering the stoichiometric equation

$$CH_6N_2 + \alpha(\beta NO_2 + \gamma N_2O_4) \rightarrow CO_2 + 3H_2O + \tfrac{9}{4}N_2$$

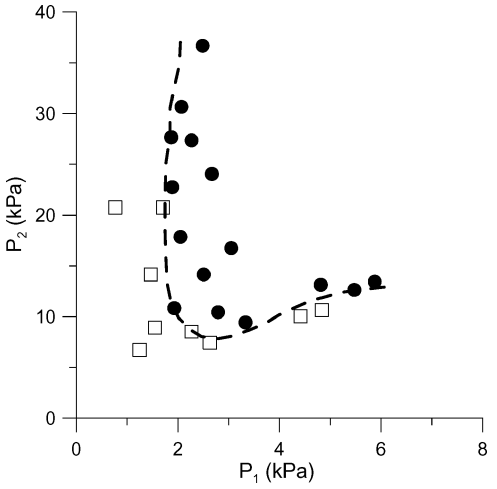

Fig. 9 NTO/MMH flammability diagram at room temperature (295 K). P_1 = mixture 60 mol% He + 40 mol% MMH. P_2 = mixture 60 mol% He + 40 mol% NTO. S/V = 48 m^{-1}. □, no ignition and ●, ignition.

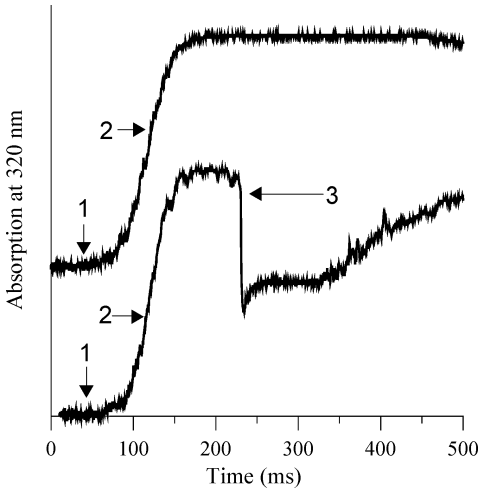

Fig. 12 NTO/MMH nonignition (top) and MMH/NTO ignition (bottom). 1, MMH absorption at 320 nm observed before NTO introduction; 2, formation of the fog and simultaneous NTO introduction in the vessel containing MMH (NTO absorbs at 320 nm) and 3, light emission at 320 nm (ignition/combustion).

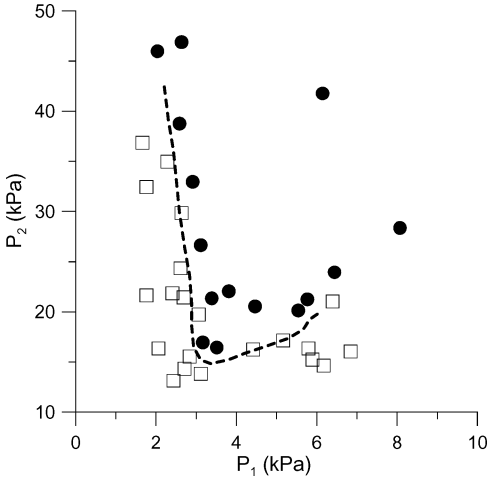

Fig. 10 NTO/MMH flammability diagram at room temperature (295 K). P_1 = mixture 70 mol% He + 30 mol% MMH. P_2 = mixture 70 mol% He + 30 mol% NTO. S/V = 48 m^{-1}. □, no ignition and ●, ignition.

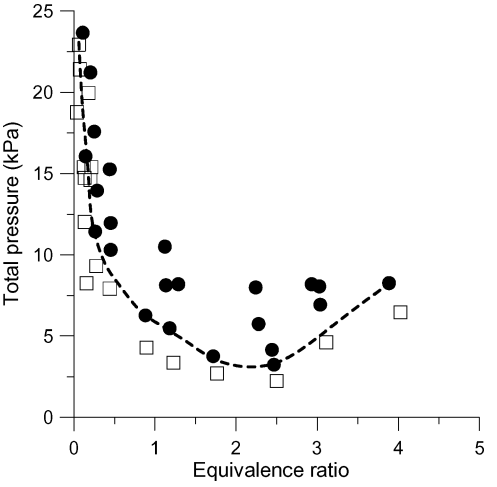

Fig. 13 Diagram total pressure–equivalence ratio obtained from Fig. 8 by assuming rapid isothermal mixing. □, no ignition and ●, ignition.

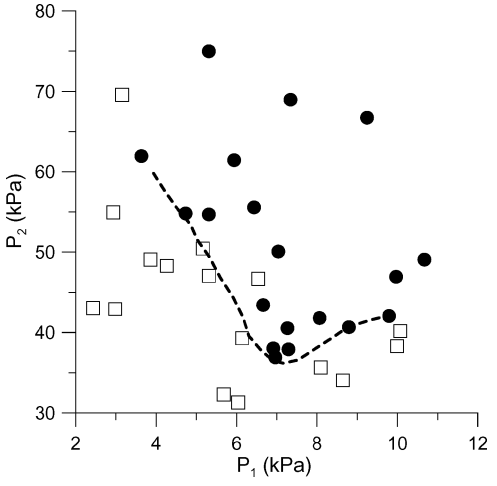

Fig. 11 NTO/MMH flammability diagram at room temperature (295 K). P_1 = mixture 80 mol% He + 20 mol% MMH. P_2 = mixture 80 mol% He + 20 mol% NTO. S/V = 48 m^{-1}. □, no ignition and ●, ignition.

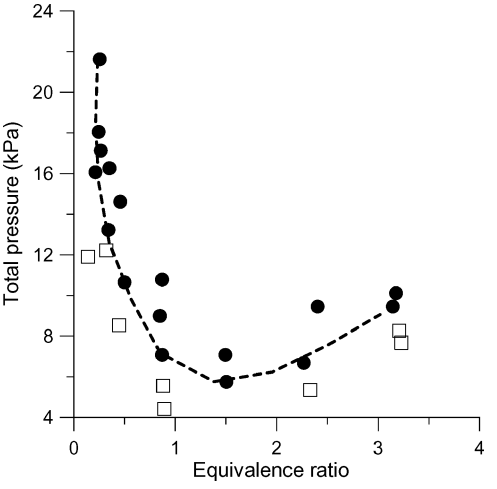

Fig. 14 Diagram total pressure–equivalence ratio obtained from Fig. 9 by assuming rapid isothermal mixing. □, no ignition and ●, ignition.

with $\alpha = \frac{5}{2}[1/(\beta + 2\gamma)]$ and $\gamma + \beta = 1$, it is possible to define the equivalence ratio Φ from the composition according to

$$\Phi = \frac{P_{\mathrm{MMH}}/P_{\mathrm{NTO}}}{1/\alpha}$$

where P_{MMH} and P_{NTO} are the partial pressures of MMH and NTO in the mixture. One can then convert the results presented Figs. 8–11 into the total pressure–equivalence ratio diagrams shown in Figs. 13–16. Figure 17 shows the total pressure–equivalence ratio diagram for mixtures containing 85 mol% helium, for which no ignition was observed in the pressure range considered here. These diagrams allow the rationalization of the experimental results obtained here. The use of the diagrams given in Figs. 13–16 is much more straightforward than for the diagrams given in Figs. 8–11, because the hazardous zone and nonhazardous zone are clearly delimited. For a given equivalence ratio in Figs. 13–16, all the mixtures at pressures above the ignition limit are unambiguously hazardous.

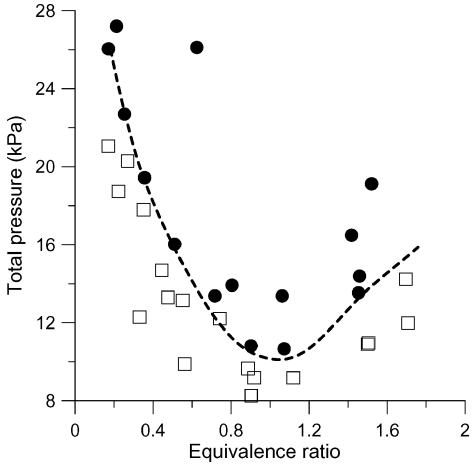

Fig. 15 Diagram total pressure–equivalence ratio obtained from Fig. 10 by assuming rapid isothermal mixing. □, no ignition and ●, ignition.

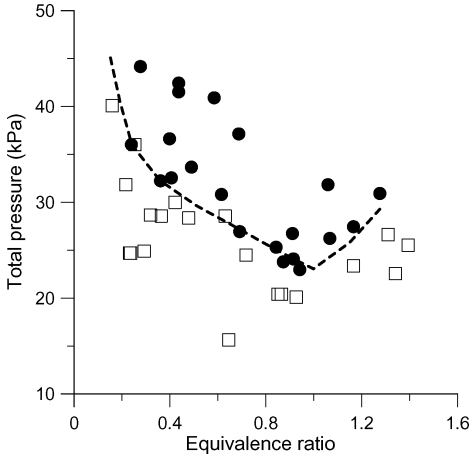

Fig. 16 Diagram total pressure–equivalence ratio obtained from Fig. 11 by assuming rapid isothermal mixing. □, no ignition and ●, ignition.

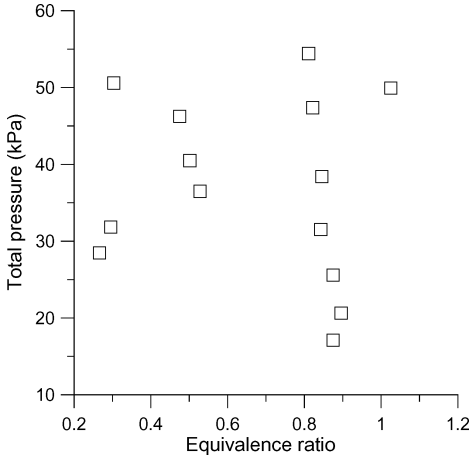

Fig. 17 Diagram total pressure–equivalence ratio obtained by assuming rapid isothermal mixing (mol% He = 85). □, no ignition.

Conclusions

The detailed chemical kinetic model proposed in a previous study is shown to be consistent with experimental features of the NTO/MMH reactivity at room temperature presented in this study. NTO/MMH/He flammability diagrams have been established. These diagrams will allow the proposal of a simple thermochemical method for the prediction of flammability diagrams for hypergolic mixtures. The experimental methods presented here can be used for investigation of environmentally compatible hypergolic fuels of the CINCH (comparative impulse noncarcinogenic hypergolics) type.

Acknowledgments

This research was supported by CNES (Centre National d'Etudes Spatiales) under Contract 2/CNES/0602 and has been conducted in the context of the HF instabilities research program (CNES, Centre National de la Recherche Scientifique, Office National d'Etudes et de Recherches Aerospatial, Société Nationale d'Etudes et de Construction de Moteurs d'Avions, Deutschen Zentrum für Luft- und Raumfahrt, ASTRIUM). L. C. wishes to thank Mark T. Swihart from the State University New York at Buffalo for editing the paper.

References

[1]Sutton, G. P., "History of Liquid Propellant Rocket Engines in the United States," *Journal of Propulsion and Power*, Vol. 19, No. 6, 2003, pp. 978–1007.

[2]Schmidt, E. W., *Hydrazine and Its Derivatives*, 2nd ed., Wiley, New York, 2001.

[3]Catoire, L., Chaumeix, N., and Paillard, C., "Chemical Kinetic Model for Monomethylhydrazine/Nitrogen Tetroxide Gas-Phase Combustion and Hypergolic Ignition," *Journal of Propulsion and Power*, Vol. 20, No. 1, 2004, pp. 87–92.

[4]Corbett, A. D., Dawson, B. E., Seamans, T. F., and Vanpee, M., "Hypergolic Ignition at Reduced Pressures," U.S. Air Force Rocket Propulsion Lab., TR-65-257, Feb. 1966.

[5]Seamans, T. F., Vanpee, M., and Agosta, V. D., "Development of a Fundamental Model of Hypergolic Ignition in Space-Ambient Engines," *AIAA Journal*, Vol. 5, No. 9, 1967, pp. 1616–1624.

[6]Daimon, W., Tanaka, M., and Kimura, I., "The Mechanisms of Explosions Induced by Contact of Hypergolic Liquid Propellants, Hydrazine and Nitrogen Tetroxide," *Proceedings of the 20th Symposium on Combustion*, The Combustion Inst., Pittsburgh, PA, 1984, pp. 2065–2071.

[7]Bassin, X., Catoire, L., Plu, E., Dupré, G., Paillard, C., and Pillet, N., "Study of the Reactivity Between Monomethylhydrazine and Nitrogen Peroxide or Oxygen in the Gaseous Phase," *Proceedings of the International Conference on Spacecraft Propulsion*, ESA and CNES, Toulouse, France, 1994, Topic 6.

[8]Mays, L. O., Farmer, M. J., and Smith, J. E., Jr., "A Laser Diagnostic Technique to Measure Chemical Delay Time in Hypergolic Combustion," *Combustion Science and Technology*, Vol. 134, Nos. 1–6, 1998, pp. 127–138.

[9]Jain, S. R., and Rajendran, G., "Chemical Aspects of the Hypergolic Preignition Reactions of Some Hybrid Hypergols," *Combustion and Flame*, Vol. 67, No. 3, 1987, pp. 207–215.

[10]Jain, S. R., and Murthy, K. N., "Temperature Profile and Ignition Delay Studies on Hypergolic Systems," *Combustion and Flame*, Vol. 81, No. 3–4, 1990, pp. 403–405.

[11]Stone, D. A., "Atmospheric Chemistry of Propellants Vapors," *Toxicology Letters*, Vol. 49, Nos. 2–3, 1989, pp. 349–360.

[12]Tuazon, E. C., Carter, W. P. L., Brown, R. V., Winer, A. M., and Pitts, J. N., "Gas-Phase Reaction of 1,1-Dimethylhydrazine with Nitrogen Dioxide," *Journal of Physical Chemistry*, Vol. 87, No. 9, 1983, pp. 1600–1605.

[13]Catoire, L., Bassin, X., Dupré, G., and Paillard, C., "Experimental Study and Kinetic Modeling of the Thermal Decomposition of Gaseous Monomethylhydrazine. Application to Detonation Sensitivity," *Shock Waves*, Vol. 6, No. 3, 1996, pp. 139–146.

[14]Catoire, L., Ludwig, T., Bassin, X., Dupré, G., and Paillard, C., "Kinetic Modeling of the Ignition Delays in Monomethylhydrazine/Oxygen/Argon Mixtures," *Proceedings of the 27th Symposium on Combustion*, The Combustion Inst., Pittsburgh, PA, 1998, pp. 2359–2365.

[15]Nonnenberg, C., Frank, I., and Klapötke, T., "Ultrafast Cold Reactions in the Bipropellant Monomethylhydrazine/Nitrogen Tetroxide: CPMD Simulations," *Angewandte Chemie International Edition*, Vol. 43, No. 35, 2004, pp. 4586–4589.

[16]Catoire, L., Ludwig, T., Dupré, G., and Paillard, C., "Kinetic Modelling of the Ignition Delays in Monomethylhydrazine/Hydrogen/Oxygen/Argon Gaseous Mixtures," *Journal of Aerospace Engineering*, Vol. 212, No. 6, 1998, pp. 393–406.

[17]Catoire, L., Bassin, X., Dupré, G., and Paillard, C., "Shock Tube Study of Ignition Delays and Detonation of Gaseous MMH/O_2 Mixtures," *Combustion and Flame*, Vol. 99, No. 3–4, 1994, pp. 573–580.

[18]Catoire, L., and Paillard, C., "Autoxidation of MMH at Room Temperature in the Gas Phase," *Reaction Kinetics and Catalysis Letters*, Vol. 69, No. 1, 2000, pp. 31–38.

[19]Mayer, S. W., Taylor, D., and Schieler, L., "Preignition Products from Propellants at Simulated High-Altitude Conditions," *Combustion Science and Technology*, Vol. 1, 1969, pp. 119–129.

[20]Breisacher, P., Takimoto, H. H., Denault, G. C., and Hicks, W. A., "Simultaneous Mass Spectrometric Differential Thermal Analyses of Nitrate Salts of Monomethylhydrazine and Methylamine," *Combustion and Flame*, Vol. 14, No. 3, 1970, pp. 397–403.

[21]Saad, M. A., Detweiler, M. B., and Sweeney, M. A., "Analysis of Reaction Products of Nitrogen Tetroxide with Hydrazines Under Nonignition Conditions," *AIAA Journal*, Vol. 10, No. 8, 1972, pp. 1073–1078.

[22]de Bonn, O., Hammerl, A., Klapötke, T. M., Mayer, P., Piotrowski, H., and Zewen, H., "Plume Deposits from Bipropellant Rocket Engines: Methylhydrazinium Nitrate and N,N-Dimethylhydrazinium Nitrate," *Zeitschrift für Anorganische und Allgemeine Chemie*, Vol. 627, No. 8, 2001, pp. 2011–2015.

[23]Perlee, H. E., Imhof, A. C., and Zabetakis, M. G., "Flammability Characteristics of Hydrazine Fuels in Nitrogen Tetroxide Atmospheres," *Journal of Chemical and Engineering Data*, Vol. 7, No. 3, 1962, pp. 377–379.

[24]Furno, A. L., Imhof, A. C., and Kuchta, J. M., "Effect of Pressure and Oxidant Concentration on Autoignition Temperatures of Selected Combustibles in Various Oxygen and Nitrogen Tetroxide Atmospheres," *Journal of Chemical and Engineering Data*, Vol. 13, No. 2, 1968, pp. 243–249.

[25]Lamoureux, N., Djebaïli-Chaumeix, N., and Paillard, C.-E., "Laminar Flame Velocity Determination for H_2-Air-He-CO_2 Mixtures Using the Spherical Bomb Method," *Experimental Thermal and Fluid Science*, Vol. 27, No. 4, 2003, pp. 385–393.